CAPILLARY PRESSURE AND RESISTIVITY MEASUREMENTS USING THE CENTRIFUGE: A NEW INTERPRETATION METHOD

Bhavani Raghuraman,* T. S. Ramakrishnan, and Michael Supp
Schlumberger-Doll Research, Old Quarry Road, Ridgefield, CT 06877

Abstract

Simultaneous in-situ measurements of resistivity and capillary pressure in a centrifuge up to speeds of 10000 rpm are reported. The setup can easily be automated for routine measurements and the electrode design takes advantage of the centrifugal force to maintain good contact between the sample and the electrodes. For converting the experimentally measured average saturations and resistivities into state properties, a new perturbation method has been developed and compared with existing methods. Capillary pressure data obtained by the centrifuge and microporous-membrane-based method show good agreement for a synthetic ceramic sample.

Introduction

While measurement of capillary pressure curves of rocks using the centrifuge is fairly common,[1-3] performing resistivity measurements in centrifuges has required the sample to be removed at every equilibrium step to make external measurements.[4] Besides being inconvenient, this may introduce errors because of saturation reversal in parts of the sample. Fluid losses resulting from sample handling are also likely. Simultaneous in-situ measurements of capillary pressure and resistivity have been reported recently.[5,6] Durand and Lenormand[5] report data up to a maximum speed of 3000 rpm using electrodes in a polymer casing on the lateral surface of the core. Because of the shape and arrangement of the electrodes it is difficult to determine a geometric factor for this setup and the analysis is further complicated by the presence of saturation gradients.

Raghuraman and Ramakrishnan[6] have proposed a design where both the average resisitivity and saturation are measured over the entire sample volume and the cell constant is known exactly. The advantages of their four electrode configuration are that it uses the centrifugal force to maintain good electrode contact with the rock and measures the average resistance of the sample over the entire length. The setup can be easily automated to make routine measurements of three samples up to speeds of 10000 rpm.

Unlike the time-consuming porous plate/membrane-based methods, the faster centrifuge technique is an indirect procedure and therefore requires additional data processing to yield the capillary pressure curve.[2,7] In this paper, we describe a new perturbation method for centrifuge data interpretation. We compare this method with other techniques

*author for correspondence

such as the Forbes' $S_{\alpha\beta}$ method[3] and Rajan's method[8] using various model capillary pressure curves.

The design of the electrodes employed here causes some bending of potential lines near the sample end faces. A commercial simulator (Maxwell EM 2D Field Simulator, ANSOFT) was used to generate the current and voltage lines in the sample and determine the error in resistivity measurements at different speeds resulting from the nonuniform electric field.

For comparative purposes we built a two-ended membrane setup similar to that described in the literature.[9] This setup gave the capillary pressure curve directly and was used to validate the data-processing algorithms for the centrifuge.

Experimental

Centrifuge setup

A modified Beckman rock core centrifuge (Model L8M/PHT) with a 10-wire slip ring (Model EC3848, Litton Poly Scientific) assembly attached to the rotor was used. A schematic of the four-terminal electrode design for a cylindrical sample is shown in Figure 1. Details of the setup have been described in an earlier publication.[6] All measurements were made at 1 kHz and 400 mV(RMS) voltage between the current electrodes. Test runs conducted with standard resistors in the cells over the entire speed range indicated good continuity and negligible noise.[6] Measurements were made on a 1.5 inch long and 0.78 inch diameter Indiana limestone (19% porosity) and a synthetic ceramic sample (45% porosity) initially saturated with 1 Ω m brine. Dodecane (99+%, Aldrich Chemicals) was used as the displacing oil phase.

Membrane-based setup

The membrane-based setup is similar to that reported in literature[9] and has a water side hydrophilic membrane (0.1 μm nylon, Sartorius) on one end face and an oil side hydrophobic membrane (0.02 μm polypropylene, Celgard 2402, Hoechst Celanese) on the other end face of the sample. The lateral surface of the 1.57 inch long and 1.5 inch diameter cylindrical sample is sealed by a viton sleeve with a pressure of 75 psig. Syringe pumps (100 DM, ISCO) on either side are used to maintain pressures, and measuring cylinders with oil-water interfaces are used to measure saturation changes in the rock. The drainage capillary pressure curve is obtained by starting with a 1 Ω m brine-saturated rock and slowly raising the capillary pressure in steps to 20 psi. The upper limit is imposed because of the possibility of breakthrough of oil through the hydrophilic membrane. At each step the saturation is measured when equilibrium is reached.

Results and Analysis

Data Interpretation: Perturbation method

The capillary pressure (p_c) at a radial distance (r) from the axis of rotation is the difference in oil and brine phase pressures at that distance in the sample. Making the usual

assumption that $p_c = 0$ at the outlet face ($r = r_2$; Figure 2), we have

$$p_c(r_1) = p_{c1} = \frac{1}{2}\Delta\rho\omega^2(r_2^2 - r_1^2) \tag{1}$$

where $\Delta\rho$ is the difference in densities of the brine and oil phases and ω is the angular velocity. The average saturation $\bar{S}$ over the sample length is then

$$p_{c1}\bar{S}(p_{c1}) = \frac{1}{2}[1 + \sqrt{1-\epsilon}] \int_0^{p_{c1}} \frac{S(p_c)\, dp_c}{\sqrt{1 - \epsilon\frac{p_c}{p_{c1}}}}\,, \tag{2}$$

where $\epsilon = 1 - r_1^2/r_2^2$. Width effects have been neglected because the Christiansen number[10] was calculated to be 0.98 for this setup. Various approximate methods have been proposed in the literature for obtaining the saturation function, $S(p_c)$, from Equation 2, the earliest of which is that of Hassler and Brunner[1] obtained with $\epsilon = 0$. Most of the subsequent approximations are either ad hoc[3,8] or numerical.[11] In contrast, our method uses a perturbation expansion, the error magnitudes of which are easily quantified, and provides a fast method to calculate $S(p_c)$.

To solve the integral equation, $\bar{S}$ is treated as a measured function of p_{c1}, and S is written in a perturbation expansion

$$S(p_{c1}) = S_0(p_{c1}) + \epsilon S_1(p_{c1}) + \epsilon^2 S_2(p_{c1}) + \epsilon^3 S_3(p_{c1}) + O(\epsilon^4)\,. \tag{3}$$

Taylor series expansions for $\sqrt{1-\epsilon}$ and $1/\sqrt{(1 - \epsilon\frac{p_c}{p_{c1}})}$ around $\epsilon = 0$, when substituted in Equation 2, gives the following explicit solutions (see Appendix A)

$$S_0(p_{c1}) = \bar{S}(p_{c1}) + p_{c1}\frac{d\bar{S}(p_{c1})}{dp_{c1}}\,, \tag{4}$$

$$S_1(p_{c1}) = \frac{1}{4}\left[\bar{S}(p_{c1}) - p_{c1}\frac{d\bar{S}(p_{c1})}{dp_{c1}}\right] - \frac{1}{2p_{c1}^2}\int_0^{p_{c1}} \gamma\bar{S}(\gamma)\, d\gamma\,, \tag{5}$$

$$\begin{aligned} S_2(p_{c1}) = {} & \frac{1}{4}\bar{S}(p_{c1}) - \frac{1}{8}p_{c1}\frac{d\bar{S}(p_{c1})}{dp_{c1}} + \frac{5 - 2\ln p_{c1}}{8p_{c1}^2}\int_0^{p_{c1}} \gamma\bar{S}(\gamma)\, d\gamma \\ & + \frac{1}{4p_{c1}^2}\int_0^{p_{c1}} \gamma\ln\gamma\bar{S}(\gamma)\, d\gamma - \frac{3}{2p_{c1}^3}\int_0^{p_{c1}} \gamma^2\bar{S}(\gamma)\, d\gamma\,, \end{aligned} \tag{6}$$

$$\begin{aligned} S_3(p_{c1}) = {} & \frac{15}{64}\bar{S}(p_{c1}) - \frac{5}{64}p_{c1}\frac{d\bar{S}(p_{c1})}{dp_{c1}} + \frac{1}{p_{c1}^2}\left(\frac{7}{16}\ln p_{c1} - \frac{1}{16}\ln^2 p_{c1} - 1\right)\int_0^{p_{c1}} \gamma\bar{S}(\gamma)\, d\gamma \\ & + \frac{21}{8p_{c1}^3}\int_0^{p_{c1}} \gamma^2\bar{S}(\gamma)\, d\gamma - \frac{45}{16p_{c1}^4}\int_0^{p_{c1}} \gamma^3\bar{S}(\gamma)\, d\gamma \\ & + \frac{1}{p_{c1}^2}\left(\frac{1}{8}\ln p_{c1} - \frac{7}{16}\right)\int_0^{p_{c1}} \gamma\ln\gamma\bar{S}(\gamma)\, d\gamma - \frac{1}{16p_{c1}^2}\int_0^{p_{c1}} \gamma\ln^2\gamma\bar{S}(\gamma)\, d\gamma\,, \end{aligned} \tag{7}$$

where $S_0(p_{c1})$ is the classical Hassler-Brunner result.[1] These solutions involve simple numerical integrations of experimentally measured quantities in addition to the traditional Hassler-Brunner calculations. In practice, although ϵ may be as high as 0.75, we find that terms up to S_3 are sufficient since the absolute magnitudes of S_1 and S_2 decrease rapidly with increasing order, as shown by our numerical investigations.

Two model capillary pressure curves were used for testing the perturbation solution using terms up to $O(\epsilon^3)$ (Figures 3a and b). The average saturation and its derivative with respect to the capillary pressure at the top face can be calculated with analytical expressions for these cases, and hence the difference between the true and predicted saturation is solely due to the error in the data inversion process. These errors were calculated as a function of the top face capillary pressure for various values of ϵ. Width effects were neglected in both the forward calculations and the inversion process. The capillary pressure curve in Figure 3a represents a gradual drop in the saturation with capillary pressure, and all three methods showed errors less than 0.01 units for ϵ values up to 0.75. The second capillary pressure curve (Figure 3b) represents a sharp drop in saturation at breakthrough pressure. Figure 4 plots the errors from data inversion for this case for three different values of ϵ. Typically, $\epsilon \leq 0.75$, and the value of 0.91 used here is an extreme test on the validity of these methods. The perturbation method shows an error spike near the breakthrough pressure (which increases with ϵ) and then monotonically reduces to zero. Rajan's method[8] is more stable near breakthrough but shows higher errors at lower saturations (high capillary pressures), leading to higher percentage errors in that region. Forbes' $S_{\alpha\beta}$ method[3] shows instabilities near breakthrough and larger offsets at lower saturations. The advantage of the perturbation method is that the error can be reduced by going to a higher order scheme. For an ϵ value of 0.75 and a capillary pressure of 2.1 psi, the error from the Forbes' method is -0.12 units. The error from a third-order perturbation solution for this case is 0.037 units, and this can be reduced to 0.025 units by going to a fourth-order scheme.

To further test these methods we generated a *discrete* data set using the model curve of Figure 3b with an ϵ of 0.75 and with no width effects. Figure 5b shows errors from the three data inversion methods. The perturbation method shows an additional spike near breakthrough; however the general trends are similar to when we use the continuous data set (Figure 4b). A second discrete data set was generated by introducing random errors in speed (10 RPM) and the fluid volume produced (0.03 cc) (Figure 5a). The errors from the perturbation technique do not fall monotonically to zero because of the random errors in the data set; however it still performs better than the other two methods (Figure 5c).

Experimental data set inversion

In an experimental data set, the average saturation data are obtained at discrete capillary pressures, and it is necessary to fit a function to these data points to facilitate differentiation and integration needed to implement any of the three methods described. Least-squares fitting of the data is common but the use of a single function to describe the entire data set can introduce errors from excessive smoothing and some of the details of the data may be lost. We have used a moving window with a three-parameter interpolating

function of the form

$$\log \bar{S}(p_{c1}) = \begin{cases} 0, & \text{below breakthrough pressure, } p_b \\ a_1 \log \frac{p_{c1}}{p_b} + a_2 \log^2 \frac{p_{c1}}{p_b} + a_3 \log^3 \frac{p_{c1}}{p_b}, & \text{otherwise.} \end{cases} \tag{8}$$

The breakthrough pressure is fixed for all the windows. Figures 6a and 9 show the estimated top face saturations for the Indiana limestone and ceramic samples. The ϵ value for our setup is 0.67 and the differences in calculated saturations are less than 1% between perturbation and Rajan's methods and 2% between perturbation and Forbes' methods.

Resistivity curves

At equilibrium, as a result of the saturation gradient, the resistivity of the rock is also nonuniform and the average resisitivity may be expressed by an equation similar to Equation 2,

$$\bar{R}(p_{c1}) = \frac{1}{2p_{c1}}[1 + \sqrt{1-\epsilon}] \int_0^{p_{c1}} \frac{R(p_c)}{\sqrt{1 - \epsilon \frac{p_c}{p_{c1}}}}\, dp_c \,. \tag{9}$$

Writing in terms of resistivity ratios gives

$$\frac{\bar{R}(p_{c1})}{R_o} = \frac{1}{2p_{c1}}[1 + \sqrt{1-\epsilon}] \int_0^{p_{c1}} \frac{R(p_c)}{R_o\sqrt{1 - \epsilon \frac{p_c}{p_{c1}}}}\, dp_c \,. \tag{10}$$

R_o is the rock resistivity at 100% saturation and is given by the Archie relation[12]

$$R = \frac{1}{\phi^m S^n} R_w \,, \tag{11}$$

for $S = 1$. Here R_w is the brine resistivity, ϕ is the rock porosity, m is the cementation exponent and n is the saturation exponent. At sufficiently low frequencies, the measured impedance, $\bar{Z}$, is equal to the sample resistance and is proportional to the average resistivity $\bar{R}$ through

$$\bar{Z}(p_{c1}) = \bar{R}(p_{c1}) \frac{l}{A} \,, \tag{12}$$

where l is the length of the rock and A is the cross-sectional area. This gives

$$\frac{\bar{R}(p_{c1})}{R_o} = \frac{\bar{Z}(p_{c1})}{Z_o} \,, \tag{13}$$

where Z_o is the measured impedance at 100% saturation. Any of the methods outlined earlier for saturation inversion may be applied to Equation 10 to obtain R/R_o from experimentally measured $\bar{R}(p_{c1})/R_o$ data.

Errors due to nonuniform fields

Because the current electrode does not cover the entire face, there is a nonuniformity in the electric field. The constant potential lines bend near the insulation and the voltage measuring electrodes (Figure 7). The error in the impedance measurement is a function of the fraction of sample face not covered by the current electrode. Because of the resistivity

gradients, the magnitude of the error could be different at different speeds. Simulations show that the error (defined as the ratio of the difference between the true and measured resistances to the true resistance) lies in the 6-8% band across the speed range of the centrifuge. Hence, while the absolute resistance measured at any one speed is lower by 6-8%, the ratio of resistance at any speed to that at 100% saturation measured using the same assembly is practically error free.

Inverting average resistance data

Figure 6b gives the experimental average resistance ratios at various top face capillary pressures for the limestone. Using procedures analogous to saturation data processing, plots of resistivity ratio as a function of capillary pressures have been obtained by the perturbation, Rajan's and Forbes' methods. Figures 8 and 10 are plots of resistivity ratio versus saturation for the limestone and ceramic samples. Using the Archie relation[12] to fit these data yields a saturation exponent of 2.2 for both the samples. However, some deviations are observed at saturations below 20-30%.

Comparing with membrane-based data

Because the centrifuge method for capillary pressure measurement is an indirect technique, it is necessary to validate this using a direct reference method such as the two-ended membrane-based method. The membrane method is extremely slow, but it directly measures capillary pressure and saturation. Figure 9 shows that the capillary pressure data from the centrifuge agrees well with the capillary pressure curves obtained from the membrane setup and from mercury porosimetry for the ceramic sample. Our membrane setup can simultaneously measure resistivities also, and experiments are being planned to compare the resistivity curves obtained by both of these techniques.

Conclusions

Simultaneous measurement of capillary pressure and resistivity in a centrifuge has been successfully demonstrated. The capillary pressure curve from the centrifuge shows good agreement with the capillary pressure curve from the membrane setup. A new data interpretation algorithm has been proposed and compared with existing techniques. Future plans include total automation of the centrifuge for routine measurements and validation of the resistivity data.

Acknowledgments

The authors thank Phil Dryden for help with sample preparation.

References

1. Hassler, G. L., and Brunner, E.: "Measurement of Capillary Pressures in Small Samples," *Pet. Trans. AIME* (1945) **160**, 114–123.
2. Ruth, D. W., and Chen, Z. A.: "Measurement and Interpretation of Centrifuge Capillary Pressure Curves-The SCA Survey," *Log Analyst* (1995) **36**, 21–33.
3. Forbes, P.: "Simple and Accurate Methods for Converting Centrifuge Data into

Drainage and Imbibition Capillary Pressure Curves," SCA Annual Technical Conference, San Antonio, Texas (1991).

4. Sprunt, E. S., Maute, R. E., and Rackers, C. L.: "An Interpretation of the SCA Electrical Resistivity Study," *Log Analyst* (1990) **31**, 76–88.
5. Durand, C., and Lenormand, R.: "Resistivity Measurements While Centrifuging," International Symposium of SCA, Calgary (1997).
6. Raghuraman, B., and Ramakrishnan, T. S.: "Simultaneous Measurement of Capillary Pressure and Resistivity using the Centrifuge," *J. Coll. Interf. Sci.* (1998) **200**, 188–191.
7. Forbes, P.: "Centrifuge Data Analysis Techniques: An SCA Survey on the Calculation of Drainage Capillary Pressure Curves from Centrifuge Measurements," International Symposium of SCA, Calgary (1997).
8. Rajan, R. R.: "Theoretically Correct Analytical Solution for Calculating Capillary Pressure - Saturation from Centrifuge Experiments," 27th Annual Logging Symposium Transactions: Society of Professional Well Log Analysts, (1986).
9. Longeron, D., Hammervold, W. L., and Skjaeveland, S. M.: "Water-Oil Capillary Pressure and Wettability Measurments Using Micropore Membrane Technique," International Symposium of SCA, Stavanger (1994).
10. Christiansen, R. L.: "Geometric Concerns for Accurate Meaurement of Capillary Pressure Relationships with Centrifuge Methods," *SPE Form. Eval.* (1992) **7**, 311–314.
11. Ayappa, K. G., Davis, H. T., Davis, E. A., and Gordon, J.: "Capillary Pressure: Centrifuge Method Revised," *AIChE Journal* (1989) **35**, 365–372.
12. Ellis, D. : *Well Logging for Earth Scientists*, Elsevier, New York (1987).

Appendix A

Perturbation algorithm

The average saturation in the sample at p_{c1} is given by

$$p_{c1}\bar{S}(p_{c1}) = \frac{1}{2}[1+\sqrt{1-\epsilon}]\int_0^{p_{c1}} \frac{S(\gamma)\,d\gamma}{\sqrt{1-\epsilon\frac{\gamma}{p_{c1}}}}\,, \tag{A1}$$

where γ is a dummy variable. Expressing S in a regular perturbation expansion with gauge functions, ϵ^n, gives

$$S(\gamma) = S_0(\gamma) + \epsilon S_1(\gamma) + \epsilon^2 S_2(\gamma) + \epsilon^3 S_3(\gamma) + O(\epsilon^4)\,. \tag{A2}$$

Using series expansions in ϵ for $\sqrt{1-\epsilon}$ and $1/\sqrt{(1-\epsilon\frac{\gamma}{p_{c1}})}$ and matching $O(\epsilon^n)$, we obtain

$$p_{c1}\bar{S}(p_{c1}) = \int_0^{p_{c1}} S_0(\gamma)\,d\gamma\,, \tag{A3}$$

$$0 = \int_0^{p_{c1}} \left(\frac{\gamma}{2p_{c1}} - \frac{1}{4}\right) S_0(\gamma)\,d\gamma + \int_0^{p_{c1}} S_1(\gamma)\,d\gamma\,, \tag{A4}$$

$$0 = \int_0^{p_{c1}} \left(\frac{3\gamma^2}{8p_{c1}^2} - \frac{\gamma}{8p_{c1}} - \frac{1}{16}\right) S_0(\gamma)\,d\gamma + \int_0^{p_{c1}} \left(\frac{\gamma}{2p_{c1}} - \frac{1}{4}\right) S_1(\gamma)\,d\gamma + \int_0^{p_{c1}} S_2(\gamma)\,d\gamma\,, \tag{A5}$$

$$0 = \int_0^{p_{c1}} \left(\frac{5\gamma^3}{16p_{c1}^3} - \frac{3\gamma^2}{32p_{c1}^2} - \frac{\gamma}{32p_{c1}} - \frac{1}{32}\right) S_0(\gamma)\,d\gamma$$

$$+\int_0^{p_{c1}}\left(\frac{3\gamma^2}{8p_{c1}^2}-\frac{\gamma}{8p_{c1}}-\frac{1}{16}\right)S_1(\gamma)\,d\gamma$$
$$+\int_0^{p_{c1}}\left(\frac{\gamma}{2p_{c1}}-\frac{1}{4}\right)S_2(\gamma)\,d\gamma+\int_0^{p_{c1}}S_3(\gamma)\,d\gamma\,, \tag{A6}$$

and so on. We now solve Equation A3 by differentiating it with respect to p_{c1} to obtain $S_0(p_{c1})$ (Equation 4). To solve for $S_1(p_{c1})$, we differentiate Equation A4 with respect to p_{c1}. This gives

$$S_1(p_{c1})=-\frac{1}{4}S_0(p_{c1})+\frac{1}{2}\int_0^{p_{c1}}\frac{\gamma}{p_{c1}^2}S_0(\gamma)\,d\gamma\,. \tag{A7}$$

We now substitute for $S_0(\gamma)$ from Equation 4. Terms that contain $\frac{d\bar{S}}{d\gamma}$ are integrated by parts and an explicit solution for S_1 can be obtained (Equation 5).

Next, Equation A5 is differentiated with respect to p_{c1} to get an expression for $S_2(p_{c1})$ in terms of S_0 and S_1, which is

$$S_2(p_{c1})=-\frac{1}{4}S_1(p_{c1})-\frac{3}{16}S_0(p_{c1})+\frac{1}{8p_{c1}^2}\int_0^{p_{c1}}\gamma\{4S_1(\gamma)-S_0(\gamma)\}d\gamma+\frac{3}{4p_{c1}^3}\int_0^{p_{c1}}\gamma^2S_0(\gamma)\,d\gamma\,. \tag{A8}$$

We again use the relationships for $S_0(\gamma)$ and $S_1(\gamma)$ to obtain

$$\int_0^{p_{c1}}\gamma S_0(\gamma)\,d\gamma=p_{c1}^2\bar{S}(p_{c1})-\int_0^{p_{c1}}\gamma\bar{S}(\gamma)\,d\gamma\,, \tag{A9}$$

$$\int_0^{p_{c1}}\gamma^2S_0(\gamma)\,d\gamma=p_{c1}^3\bar{S}(p_{c1})-2\int_0^{p_{c1}}\gamma^2\bar{S}(\gamma)\,d\gamma\,, \tag{A10}$$

and

$$\int_0^{p_{c1}}\gamma S_1(\gamma)\,d\gamma=\frac{1}{4}\int_0^{p_{c1}}\gamma\left\{\bar{S}(\gamma)-\gamma\frac{d\bar{S}(\gamma)}{d\gamma}\right\}d\gamma-\frac{1}{2}\int_0^{p_{c1}}\frac{1}{\gamma}\,d\gamma\int_0^{\gamma}\beta\bar{S}(\beta)\,d\beta\,, \tag{A11}$$

where β is again a dummy variable. The double integral may be simplified through integration by parts and recognizing that

$$\int_0^{p_{c1}}\frac{1}{\gamma}\,d\gamma\int_0^{\gamma}\beta\bar{S}(\beta)\,d\beta=\ln p_{c1}\int_0^{p_{c1}}\gamma\bar{S}(\gamma)\,d\gamma-\int_0^{p_{c1}}\gamma\bar{S}(\gamma)\ln\gamma\,d\gamma\,, \tag{A12}$$

since $\lim_{\gamma\to0}\ln\gamma\left(\int_0^{\gamma}\beta\bar{S}(\beta)\,d\beta\right)=0$. The final result for $S_2(p_{c1})$ is then given by Equation 6. The analysis may now be continued ad infinitum to higher orders.

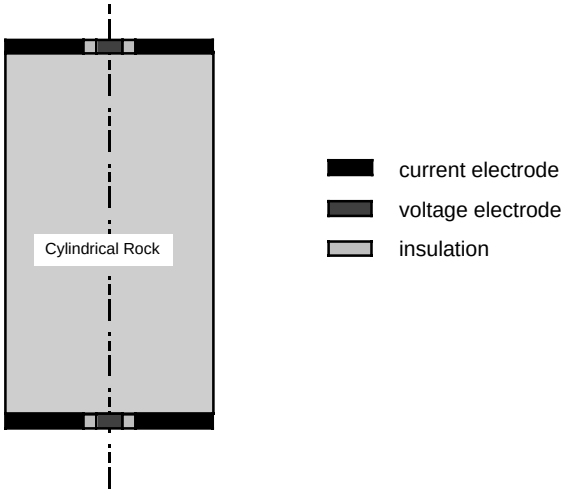

Fig. 1: Schematic of electrode geometry

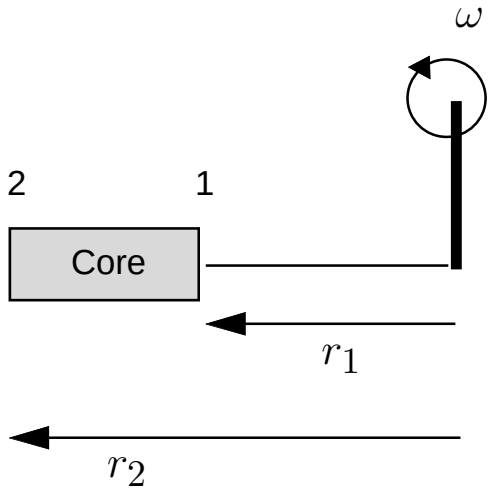

Fig. 2: Schematic of centrifuge geometry

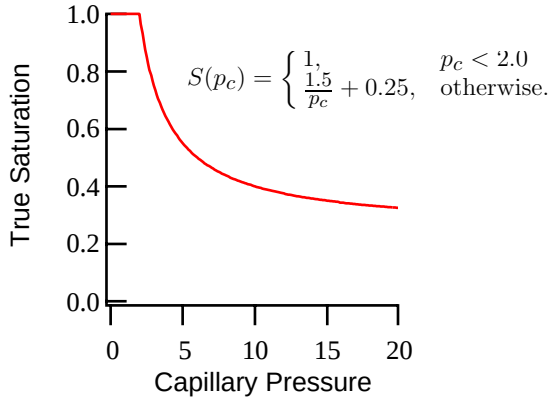

(a)

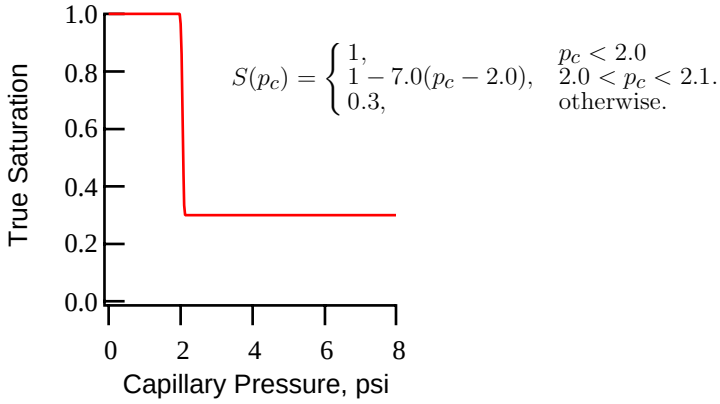

(b)

Fig. 3: Model capillary pressure curves used for testing data processing methods.

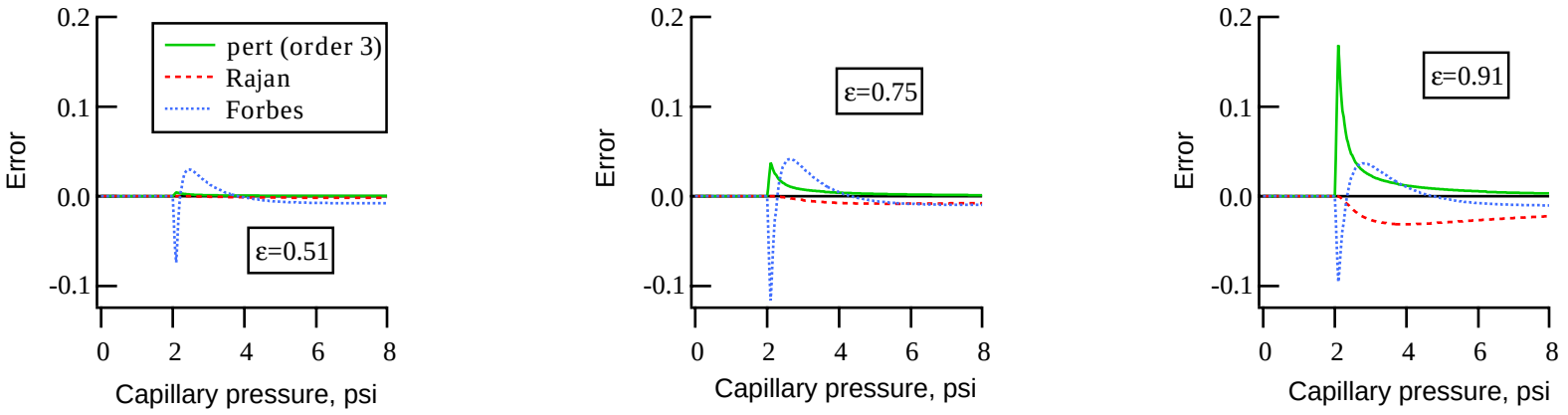

(a) (b) (c)

Fig. 4: Calculated errors for model curve in Fig. 3b using perturbation, Rajan's and Forbes' methods. Errors increase with increasing ε; however, the offset from the perturbation method falls to zero at high pressures. ε =0.91 is an extreme case, not observed in practical centrifuges. Perturbation errors can be reduced by going to higher orders. Error is defined as the difference between the true and predicted saturations.

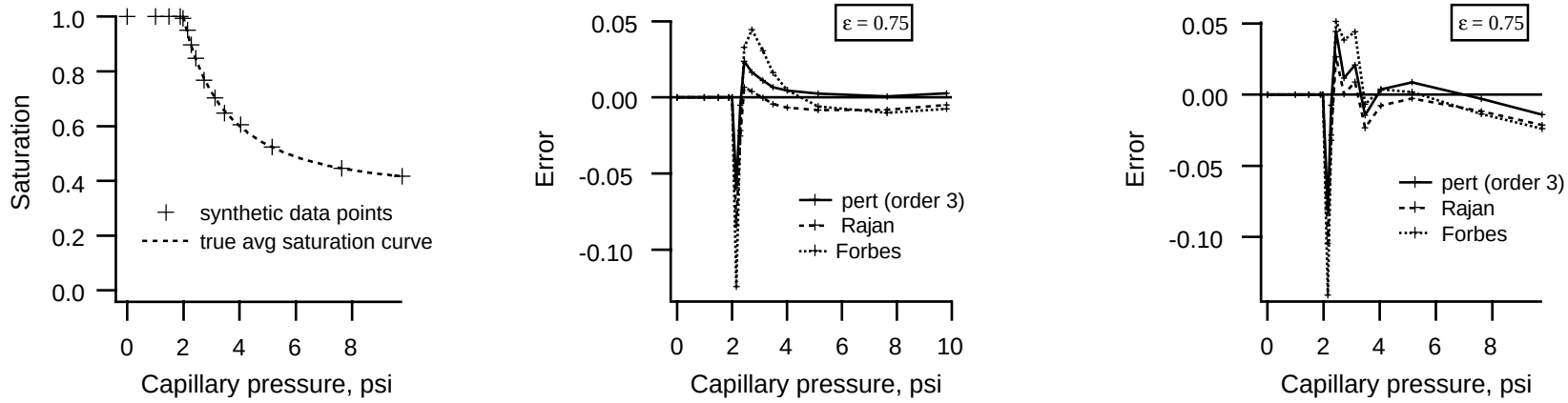

(a) (b) (c)

Fig. 5: (a) Synthetic experimental data set generated for model curve of Fig. 3b. (b) Errors with the discrete data set. (c) Errors in processing when discrete data set includes random errors in RPM and fluid volume. Pore volume of sample is taken to be 2.5 cc.

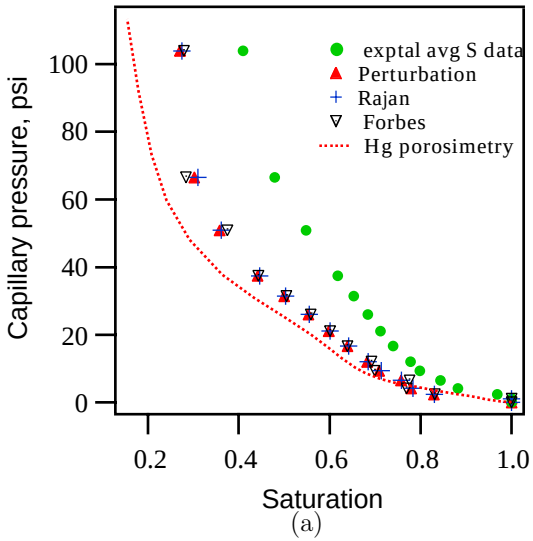

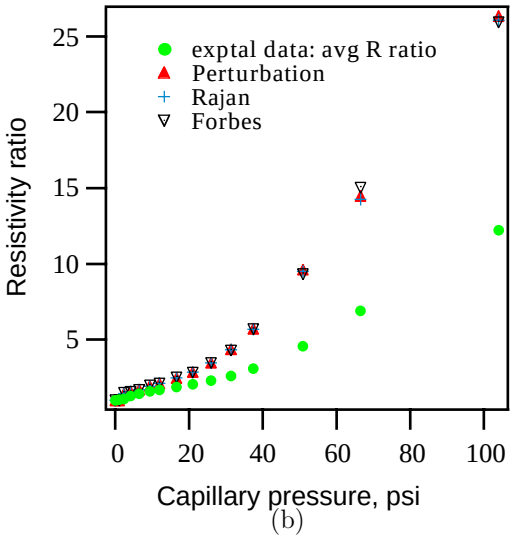

Fig. 6: (a) Capillary pressure and (b) resistivity ratio curves for Indiana limestone. Curves obtained by inverting average experimental data using various algorithms.

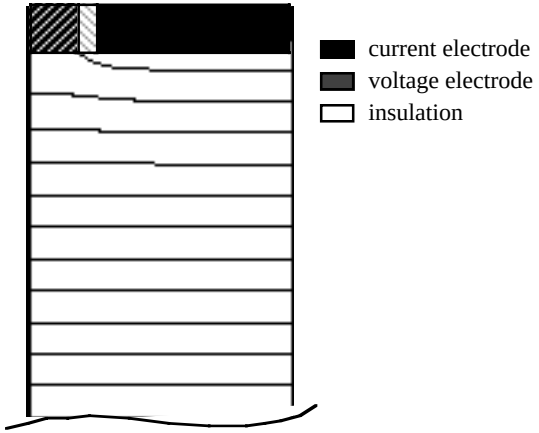

Fig. 7: Equipotential contours for the electrode geometry used in the setup. Potential within any electrode is uniform.

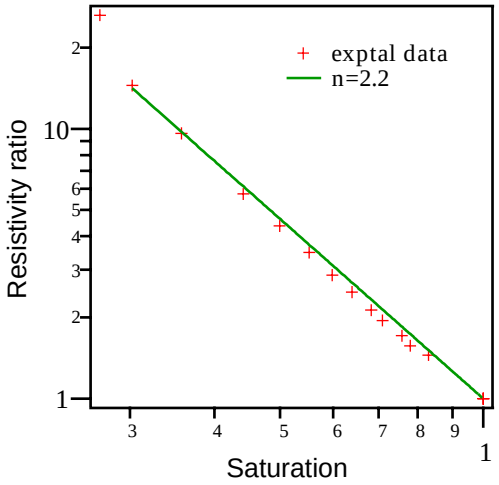

Fig. 8: Resistivity ratio curve for the limestone. Archie fit gives a saturation exponent of 2.2.

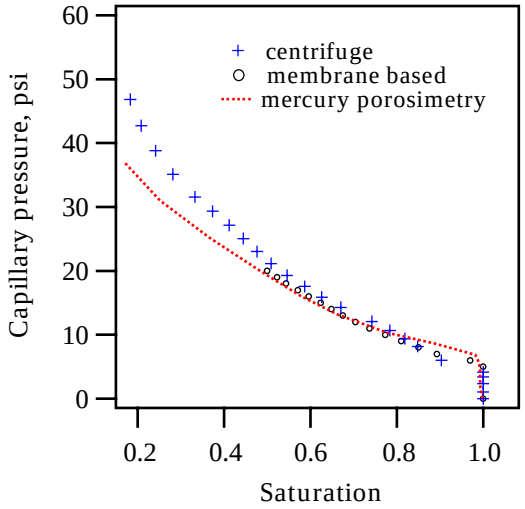

Fig. 9: Capillary pressure curve for the ceramic sample using the perturbation method. Good agreement is observed with the curve from the membrane method.

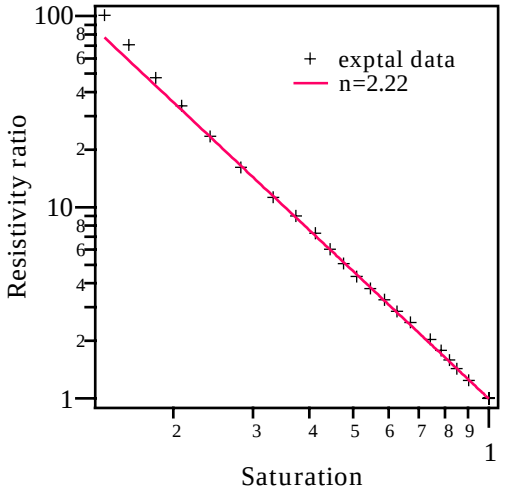

Fig. 10: Resistivity ratio curve for the ceramic. Archie fit gives a saturation exponent of 2.2.